J. Fluid Mech. (2017), *vol.* 829, *pp.* 459–485.
doi:10.1017/jfm.2017.543

Experiments on, and discrete and continuum simulations of, the discharge of granular media from silos with a lateral orifice

Y. Zhou[1,2], P.-Y. Lagrée[3], S. Popinet[3], P. Ruyer[1] and P. Aussillous[2,†]

[1]Institut de Radioprotection et de Sûreté Nucléaire (IRSN), PSN-RES, SEMIA, LIMAR, Cadarache, St Paul-Lez-Durance, 13115, France

[2]Aix-Marseille Univ, CNRS, IUSTI, Marseille, France

[3]Sorbonne Universités, UPMC Univ Paris 06, CNRS UMR 7190, Institut Jean le Rond ∂′Alembert, F-75005 Paris, France

(Received 15 November 2016; revised 18 May 2017; accepted 2 August 2017; first published online 21 September 2017)

We compare laboratory experiments, contact dynamics simulations and continuum Navier–Stokes simulations with a $\mu(I)$ visco-plastic rheology, of the discharge of granular media from a silo with a lateral orifice. We consider a rectangular silo with an orifice of height D which spans the silo width W, and we observe two regimes. For small enough aperture aspect ratio $\mathcal{A}=D/W$, the Hagen–Beverloo relation is obtained. For thin enough silos, $\mathcal{A}\gg\mathcal{A}_c$, we observe a second regime where the outlet velocity varies with $\sqrt{W}$. This new regime is also obtained in the continuum simulations when the friction on side walls is taken into account in a thickness-averaged version of $\mu(I)$ + Navier–Stokes (in the spirit of Hele-Shaw flows). Moreover most of the internal details of the flow field observed experimentally are reproduced when considering this lateral friction. These two regimes are recovered experimentally for a cylindrical silo with a lateral rectangular orifice of height D and arc length W. The dependency of the flow rate on the particle diameter is found to be reasonably described experimentally using two geometrical functions that depend respectively on the number of beads through the two aperture dimensions. This is consistent with two-dimensional discrete simulation results: at the outlet, the volume fraction and the velocities depend on the particle diameter and this behaviour is correctly described by those geometrical functions. A similar dependency is observed in the two-dimensional continuum simulations.

Key words: complex fluids, granular media

1. Introduction

Discharge of granular media out of a silo through an aperture is a classical problem with many practical and industrial applications. The main scaling relation, generally known as the Hagen–Beverloo relation, predicts that the mass flow rate scales as $(D-kd)^{5/2}$ where D is the diameter of the aperture, d the grain size and k an empirical

†Email address for correspondence: pascale.aussillous@univ-amu.fr

parameter. However detailed understanding of the physical processes leading to such a scaling is still lacking (Janda, Zuriguel & Maza 2012; Perge *et al.* 2012). Numerical simulations that explicitly solve granular media at the scale of the particle, such as discrete element methods, can provide detailed and promising insight into the flow. On the other hand, rheological models able to describe the flow at the scale of its opening are still under development.

The Hagen–Beverloo scaling implies that, as long as the silo dimensions are sufficiently larger than the aperture scale, the geometry of the silo and its walls are irrelevant for the determination of the flow rate. However the conditions for which this statement holds are still unclear: what are the criteria that bound this behaviour and what are the control parameters that drive the flow beyond the classical regime? The present study aims to study this departure for a specific case of industrial relevance. Let us consider a non-classical geometrical configuration of the reservoir containing the granular medium: a vertical and elongated cylindrical tube of diameter of the order of centimetres with a lateral opening of similar size. This case is of particular interest to understand conditions under which solid fuel particles inside a typical pressurised-water nuclear reactor fuel rod, whose cladding would have failed under hypothetical accidental conditions, could disperse out of this rod. The fuel particles are generated from an initially cylindrical pellet (scale of centimetres) that can be fragmented due to the irradiation process (burn up of the fuel) or accidental conditions (large pressure and temperature variations inside the rod). The size distribution of the fragments can be wide, the smallest size being of the order of 10 μm. In this study the particles are composed of a population of spherical beads and are monodisperse in diameter. Therefore, the probability of jamming and arch formation throughout the silo is as low as possible due to the small contact area between neighbouring particles. The discharge flow is therefore believed to overestimate that of a more realistic granular material of the same average size. This granular reservoir has two main peculiarities in regard to more classical hopper geometries. Firstly, for a given cross-section of the flow, the perimeter over which wall friction occurs is relatively large (by analogy, one could talk of a small hydraulic diameter) which raises the question of the possible impact of wall friction on the flow rate. Secondly, the aperture is vertical, an orientation that necessarily impacts the discharge for a gravity-driven flow. Moreover, the number of beads through the aperture can vary over a large range and is known to have a large effect at low values of flow rate.

The impact of the angle of the aperture surface (relative to horizontal) on the discharge flow rate of a silo (a so-called tilted hopper) has been already studied experimentally. For beads, (Sheldon & Durian 2010) or sand and sugar, Medina *et al.* (2014) and Serrano *et al.* (2015) recovered a flow rate scaling as $D^{5/2}$, as long as clogging did not occur (which is only slightly affected by a vertical orientation of the aperture). According to the authors, the success of the Hagen–Beverloo scaling in this configuration indicates that one of the classical physical interpretations of the relation in terms of free fall under an arch of aperture size is questionable. The shape and size of the aperture were varied, but the size of the aperture was always small compared to the silo width, which does not cover our range of interest. The wall thickness of the silo can alter the discharge flow rate of tilted hoppers as soon as it is sufficiently wide, according to Medina *et al.* (2014) and Serrano *et al.* (2015). In these studies, the thickness was varied between zero and approximatively half the aperture size, the latter always being an order of magnitude larger than the typical grain size. In our case the typical cladding of a nuclear fuel rod is less than 1 mm thick and the experimental facility has been designed to avoid any impact of wall

thickness on the discharge rate. In those studies, the number of grains in the aperture were varied solely by varying the aperture size, the grain size remaining constant. Sheldon & Durian (2010) also underlined the possible influence of the hopper wall as being an interesting line for future research.

As long as the granular bed height inside the silo is larger than its width, the discharge flow rate does not depend on this height, a useful property used historically for time measurement with sandglasses. This has some similarity to the so-called Janssen effect that is observed for static packing of granular material confined by vertical walls. During the discharge, relative motion of the granular material with respect to these walls has to be considered and Bertho, Giorgiutti-Dauphiné & Hulin (2003) have shown that the Janssen effect can be recovered in this configuration. However, Aguirre *et al.* (2010) have shown that the Janssen effect (i.e. the pressure level at the outlet) does not influence the granular discharge flow rate. The frictional interaction of flowing granular material with walls and its possible influence on the discharge flow rate for our geometry is therefore an open question.

For a small number of grains through the aperture, the flow rate depends on grain size (the larger the size, the lower the flow rate). The Hagen–Beverloo relation includes this effect. One of the classical interpretations of this d dependency is the existence of an empty annulus that reduces the effective aperture area for the granular flow. But recent studies of the velocity and density profiles of the granular flow over horizontal apertures, e.g. Janda *et al.* (2012), indicate that the number of grains through the aperture is strongly correlated to the dilatancy of the flow over the entire flow cross-section (and not only over its periphery). There is therefore interest in generalising this statement for other flow configurations where the Hagen–Beverloo relation holds, like the case of vertical aperture of interest in our study.

We present an investigation of the discharge flow rate of a granular material of spherical glass beads of variable size confined in a vertical elongated silo of variable shape and size, with a lateral aperture also of variable shape and size, while neglecting the effect of the wall thickness. The methods used are first introduced in § 2. The main scaling relations that could be deduced from dimensional analysis (see § 3.1) are recovered by the set of experiments performed (see § 3.2). It is then shown that the influence of the silo geometry on the flow rate can be simulated thanks to a continuum model for the granular flow with a frictional rheology described by a $\mu(I)$ constitutive law (where the frictional coefficient μ depends on the inertial number I) and taking into account the wall friction (§§ 3.3 and 3.4). The observed influence of the beads size on the flow rate is analysed in terms of dilatancy over the aperture cross-section: experimental results trends are supported by contact dynamics simulations of the flow through a vertical aperture (see § 3.5).

2. Methods

2.1. *Experiments*

Two geometries of silos have been considered, either rectangular or cylindrical, as shown in figure 1(*a*,*b*). The typical height H of the silos is larger than 500 mm, that is always one order of magnitude larger than its lateral extent. The lateral extent of the rectangular silo and the diameter of the cylindrical silo are fixed to 60 mm and 40 mm respectively. The aperture on the lateral side wall has a rectangular shape with a height D and a horizontal length W. For rectangular silos, W is also the width of the silo. For cylindrical silos, W is the orifice arc length. The whole set of geometrical data considered in this study is given in table 1. The back wall of the rectangular silo

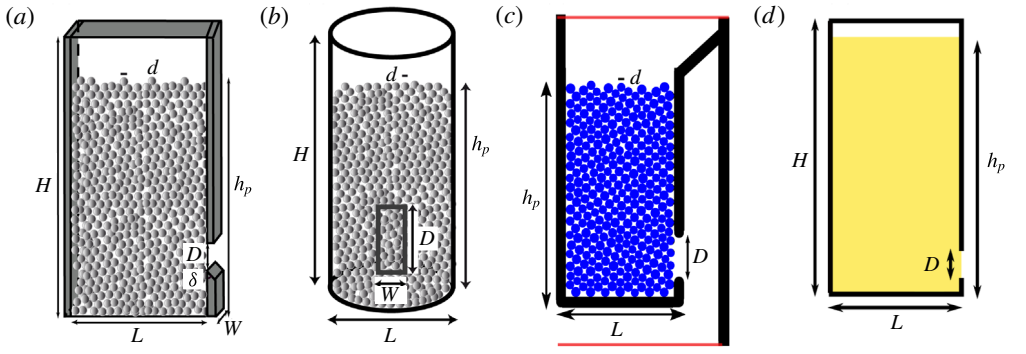

FIGURE 1. (Colour online) Schematic apparatus of the silo. (*a*) Experimental rectangular silo. (*b*) Experimental cylindrical silo. (*c*) Two-dimensional (2-D) discrete simulation. (*d*) Continuum simulation. The horizontal red lines in (*c*) represent the horizontal boundaries of the computational domain.

	D	W	d
Exp. Rect. silo	[2.7, 5.4, 10, 15 20, 25, 30, 35] mm	[3.5, 5, 10, 20 30, 40] mm	[124, 190, 375, 538 762, 1129, 1347] μm
Exp. Cyl. silo	[5, 10, 20, 25, 30 35, 40, 41.5] mm	[5, 10.1, 15.4, 20.9 33.9, 62.8] mm	[124, 190, 375, 538 762, 1129, 1347] μm
Discrete 2-D sim.	[6, 8, 10, 12 14, 16, 18, 20] d	—	[2, 6] mm
Continuum 2-D sim.	[0.4375, 0.5, 0.5625, 0.625 0.6562, 0.6875, 0.75] L	—	$L/30$, $L/90$
Continuum pseudo-3-D sim.	[0.4375, 0.5, 0.5625, 0.5938 0.625, 0.6562, 0.6875, 0.75] L	[0.16, 0.2, 0.25 0.5, 1, 2] L	$L/30$, $L/90$

TABLE 1. Performed runs, the dimensions are defined in figure 1.

is made of a copper frame connected to ground to discharge static electricity. Front, bottom and lateral walls of the rectangular silo, as well as cylindrical walls, are made of a Plexiglas frame of millimetre width. The walls have been bevelled along the aperture with an angle δ, as represented in figure 1. A preliminary study has shown that the discharge flow rate was independent from this angle (and therefore that the friction along the wall thickness was negligible) as long as $\delta < 60°$. The value $\delta = 30°$ has been chosen. The bottom of the aperture is at a vertical distance larger than 20 mm from the bottom of the silo (corresponding to at least 15 layers of beads): lower values affect the discharge rate.

The non-cohesive spherical glass beads of density $\rho = 2500$ kg m^{-3} (Potter & Ballotini Inc.) have been sifted between $0.9d$ and $1.1d$, with d the mean diameter. The initial (before the opening of the aperture) volume fraction of particles in the silo ϕ_b has been estimated from the initial mass (of granular material before filling) and from the initial height h_p within the silo. During the discharge, the grains flowing through the aperture are collected and their mass is measured with an electronic balance (Mettler Toldeo 6002S) with an accuracy of 0.1 g and a frequency of 20 Hz. We observed a steady-state discharge regime for all the configurations explored. From the slope of the collected mass evolution during

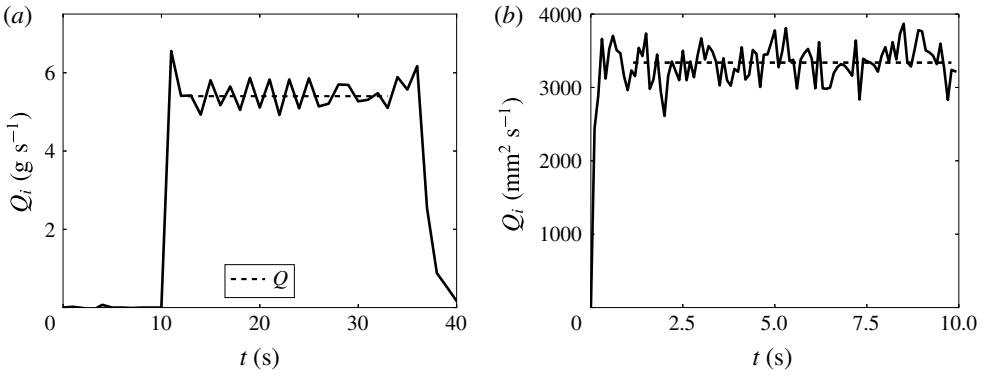

FIGURE 2. Temporal evolution of the instantaneous flow rate. (*a*) Experiment with rectangular silo, $d = 190$ μm, $D = 10$ mm and $W = 3.5$ mm. (*b*) Two-dimensional discrete simulation with $d = 2$ mm and $D = 16$ mm. The dashed lines represent the mean flow rate Q.

this regime, one deduces the instantaneous mass flow rate, Q_i, and the mean flow rate, Q, as displayed in figure 2(*a*). The data are available as supplementary material at https://doi.org/10.1017/jfm.2017.543. A Photron high-speed optical camera FASTCAM APX RS has been used during rectangular silo discharge with a spatial resolution of 256×1024 pixels^2, a frequency of acquisition of 250 Hz with a SIGMA zoom 24–700 mm f2.8. Using the DPIVsoft software (Meunier & Leweke 2003) we performed particle image velocimetry (PIV) of the granular flow and were able to get streamlines and 2-D velocity fields at the front wall of the silo (as illustrated in figure 7). Using an interface tracking algorithm, the instantaneous profile of the upper layer of beads in the silo has also been recorded (as illustrated in figure 11).

2.2. *Contact dynamics simulations*

Following the work of Zhou, Ruyer & Aussillous (2015) we used the LMGC 90 software implementation of the contact dynamics method (Radjai & Dubois 2011) to study the discharge of a silo with a lateral orifice. As discrete simulations in three dimensions are too demanding given our computational resources, we only performed 2-D simulations, which still take hours or even days. The two-dimensional silo (figure 1*c*) consists of a rectangular reservoir, of width L, filled with a height h_p of particles of mean size d. There is a dispersion $\delta d/d = 0.2$ in the size of the particles to avoid crystallisation. The wall thickness is imposed to be equal to the diameter of the biggest particle in the silo, d_M, with a circular shape at the edge of the outlet. The outlet is located at the side, $3.5d_M$ above the bottom, and has a length D which was varied. The circular particles are treated as perfectly rigid and inelastic and contact dissipation is modelled in terms of a friction coefficient that we set to $\mu_p = 0.4$ between particles, and $\mu_w = 0.5$ between the particles and the wall. The number of particles, reported in table 2, was chosen for each simulation to ensure that the discharge flow rate is independent from the column height with $16D < H < 45D$. To ensure that the lateral walls do not influence the flow significantly, we impose a width of the silo $L = 3D$. The granular column is prepared by the random deposition of particles in the closed silo. The initial volume fraction of particles in the silo ϕ_b has been measured in the central zone of the silo. Simulations are then run with a

	$d=2$ mm		$d=6$ mm	
D/d	N_p	N_t	N_p	N_t
6	5 000	30 000	4 000	30 600
8	7 500	20 000	5 400	22 000
10	10 000	20 000	8 400	20 000
12	11 290	16 000	12 000	20 000
14	13 500	15 000	14 000	16 000
16	15 500	10 000	16 000	9 200
18	20 000	5 200	18 000	8 000
20			20 000	6 000

TABLE 2. Parameters used in discrete simulations for given particle sizes ($d=2$ mm and $d=6$ mm), where N_p is the number of particles and N_t is the number of time steps.

time step of $\delta t = 5 \times 10^{-4}$ s and for a number of time steps N_t reported in table 2. The computational domain is periodic in the vertical direction to keep a constant number of particles. The horizontal boundaries of the computational domain are set at a distance $10d_M$ below, and $30d_M$ to $70d_M$ above the silo (see the red horizontal lines in figure 1*c*).

Figure 2(*b*) shows a typical temporal evolution of the instantaneous flow rate. The flow rate is found to rapidly reach a stationary value Q. The output data at the aperture line are time averaged during this steady-state regime of discharge to deduce the vertical profiles of velocity and particle volume fraction. Further details may be found in Zhou *et al.* (2015).

2.3. *Continuum numerical simulations*

2.3.1. *General equations*

We turn to the continuum simulation method in the framework of the $\mu(I)$-rheology, a non-Newtonian rheology for granular flows proposed by Midi (2004) and Jop, Forterre & Pouliquen (2006). The non-Newtonian incompressible Navier–Stokes system reads:

$$\boldsymbol{\nabla}\cdot\boldsymbol{u}=0, \tag{2.1}$$

$$\rho\left(\frac{\partial \boldsymbol{u}}{\partial t}+\boldsymbol{u}\cdot\boldsymbol{\nabla}\boldsymbol{u}\right)=-\boldsymbol{\nabla}p+\boldsymbol{\nabla}\cdot(2\eta\boldsymbol{D})+\rho\boldsymbol{g}+\boldsymbol{f}_w, \tag{2.2}$$

where $\boldsymbol{D}$ is the strain-rate tensor $(\boldsymbol{\nabla}\boldsymbol{u}+\boldsymbol{\nabla}\boldsymbol{u}^{\mathrm{T}})/2$ and $\boldsymbol{f}_w$ is a volumetric force (discussed in § 2.3.3). Following Jop, Forterre & Pouliquen (2005), the $\mu(I)$ viscosity is an effective viscosity η depending both on the shear rate (the inertial number I being proportional to the second invariant D_2 of the strain-rate tensor $D_2=\sqrt{D_{ij}D_{ij}}$) and the local pressure. It reads:

$$\eta=\frac{\mu(I)}{\sqrt{2}D_2}p, \quad \text{with } I=\frac{d\sqrt{2}D_2}{\sqrt{p/\rho}}, \quad \text{and} \quad \mu(I)=\mu_s+\frac{\Delta\mu}{I_0/I+1}. \tag{2.3a–c}$$

We take for the rheological constants $\mu_s=0.4$, $\Delta\mu=0.28$ and $I_0=0.4$, but we do not consider the variation of the volume fraction with I given by Jop *et al.* (2006), as we suppose the flow incompressible. At the solid boundaries we impose a no-slip condition. Pressure is zero at the orifice. In the original model pressure is zero at the

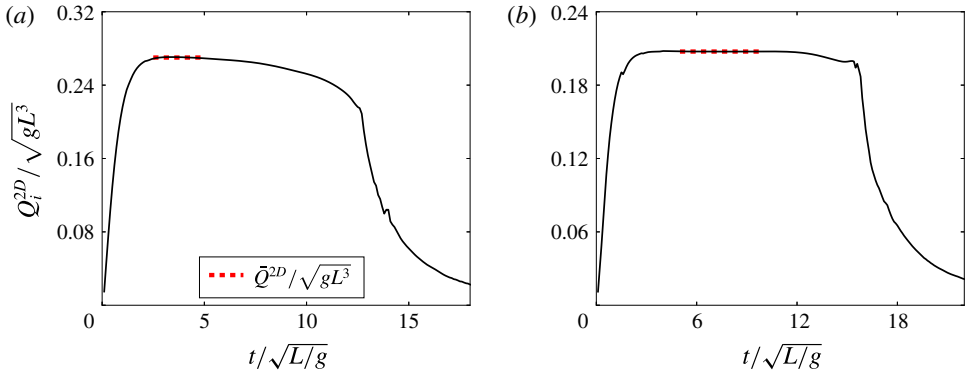

FIGURE 3. (Colour online) Continuum simulation: temporal evolution of the dimensionless instantaneous flow rate $Q_i^{2D}/(\sqrt{gL^3})$, as a function of the dimensionless time $t/\sqrt{L/g}$ for $L = 90d$ and $D = 0.5L$ (*a*) in two dimensions (*b*) in pseudo three dimensions with $W = 22.5d$. The dashed lines represent the mean flow rate $Q^{2D}/(\sqrt{gL^3})$.

free surface. To simplify the implementation of this boundary condition for a moving free surface, we introduce a second passive fluid of small density and viscosity and impose the zero pressure condition along the top boundary of the domain.

The Navier–Stokes simulations are performed with the free software *Basilisk* (Popinet 2013–2016), which is the successor of *Gerris* (Popinet 2003, 2009) and uses a similar finite-volume projection method. Two phases are present, a surrounding gas and the granular fluid. The interface between these two phases is tracked with a volume-of-fluid method. The viscosity and density of the surrounding gas are small, so that the latter's influence on the granular flow is minimised. The computational cost is dominated by the solution of two Poisson–Helmholtz problems: a scalar Poisson equation for the pressure necessary to enforce incompressibility and a vector Poisson–Helmholtz equation for the time-implicit discretisation of the viscous term. Note that in contrast with the formulation in *Gerris* Lagrée, Staron & Popinet (2011), the fully coupled Poisson–Helmholtz problem for the velocity is solved (including coupling terms between velocity components). The simulations in this paper are in two dimensions. The CPU time of each simulation is always less than one hour on a laptop computer. (The full code used is available and commented here: http://basilisk.fr/sandbox/M1EMN/Exemples/granular_sandglass_muw.c.) We use a regularisation technique to avoid the divergence of the viscosity when the shear becomes too small by replacing η by $\min(\eta, \eta_{max})$ with $\eta_{max} = 100$ a constant large enough, as done successfully in Lagrée *et al.* (2011) and Staron, Lagrée & Popinet (2012, 2014) where further details on the numerical method can be found.

2.3.2. *Pure 2-D configuration*

We consider a two-dimensional silo of width L, along the x axis, (gravity $\boldsymbol{g}$ is along negative y axis) initially filled with a height $h_p = 3.9L$ of the visco-plastic fluid (see figure 1*d*). The mesh is such that the width of the silo L is divided in 64 computation cells which is a good balance between precision and computational time.

We first performed a series of simulations in the two-dimensional case, imposing $\boldsymbol{f}_w = 0$. We varied the size of the aperture D and the particle diameters (see table 1). In figure 3(*a*), the instantaneous flow rate obtained for a given run, Q_i^{2D}, is found

to be close to stationary during the discharge as in the experiments. As done in the experiments, we measure the mean flow rate, Q^{2D}, in the stationary regime (dashed lines in the figure).

2.3.3. *Averaged 2-D or pseudo-3-D configuration*

To take into account the lateral friction on the walls and mimic 3-D effects, we average the momentum equation across the width of the silo in the spirit of Hele-Shaw flows, Jop *et al.* (2005) and Lagrée (2007). For pure Hele-Shaw flows (with a Newtonian viscous fluid), the velocity is supposed to have a parabolic profile in the transverse z direction. Here we suppose that the shape of the profile is almost flat, which reflects the yield-stress nature of the granular fluid. Hence the term appearing in front of the nonlinear derivative term associated with the effective chosen profile is unity (see Lagrée 2007, for a discussion of the classical viscous case and bibliography). The integration of the viscous force across the cell gives the contribution of the friction stress at the wall, supposed to be a Coulomb force again: $-\mu_w p$ on each wall. This wall friction acts in the direction of the velocity. This gives the average additional force from the side walls in the momentum equation,

$$\boldsymbol{f}_w = -2\frac{\mu_w p}{W}\frac{\boldsymbol{u}}{|\boldsymbol{u}|}. \tag{2.4}$$

From a Hele-Shaw point of view, the momentum (2.2) and incompressibility (2.1) equations apply to a 2-D-averaged velocity field (u, v), with the extra source term in the momentum (2.2) taking into account the wall friction (2.4). We chose the value $\mu_w = 0.1$ and varied the pseudo-width W, together with the aperture length D, and the particle diameter d, as shown in table 1. Note that in the simulations $2L\mu_w/W$ is the effective parameter. To compare with experiments and discrete dynamics (where the natural scale is d), the geometrical parameters of the continuous simulations are scaled by d (see labels of figures 7 and 11).

In these pseudo-3-D simulations, the different fields (velocity, pressure) are interpreted as width averages. The instantaneous flow rate is again found to be stationary during the discharge (figure 3*b*). We measured the mean flow rate Q^{2D} in the stationary regime (see the dashed lines in the figure) and we defined the equivalent 3-D flow rate as $Q = WQ^{2D}$.

Note that when the friction at the wall $\boldsymbol{f}_w$ were too large, the continuum simulations failed. We varied $2L\mu_w/W$ up to about 5.6, but were not able to reach larger values. Further developments have to be done to overcome this problem, which could be related to the numerical method. Nonetheless the range of W covered is sufficient to compare qualitatively the results of the simulations with the experiments.

3. Effect of side walls on the silo discharge from a lateral orifice

The aim of this study is to clarify the role of the two dimensions of the outlet, the height D and the width W as defined in figure 1, in the discharge of a silo from a lateral aperture. In a first part we have simplified the problem by considering a rectangular silo where the orifice spans the width of the silo. We first present the experimental results. We then discuss the role of the side walls on the flow rate using continuum simulations. Finally we extend the result to the cylindrical silo and we discuss the role of the particle diameter.

3.1. Π *theorem*

The mass flow rate out of the silo, Q, depends on the density ρ, the gravity g and the geometrical parameters: width L, orifice height D, thickness W, the filling height

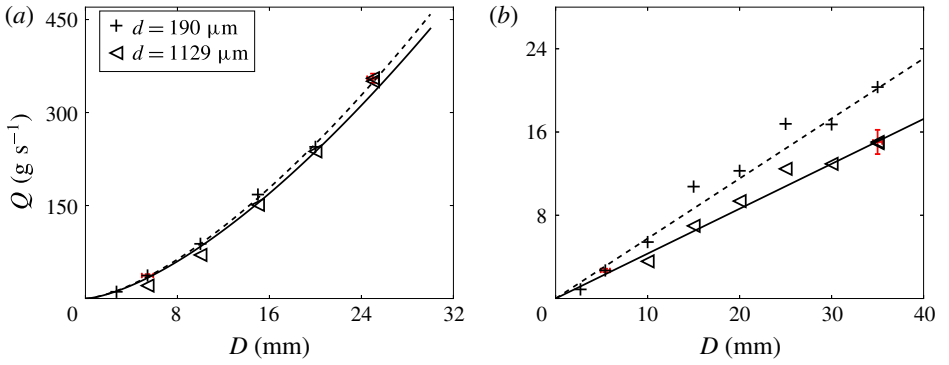

FIGURE 4. (Colour online) Experimental mass flow rate Q in the rectangular silo versus the height of orifice D for two sizes of particles d. (*a*) $W = 40$ mm, the dashed (respectively full) line represents the equation $Q = c_1 D^{3/2}$ where $c_1 = 2.79$ g s^{-1} mm$^{-3/2}$ (respectively $c_1 = 2.65$ g s^{-1} mm$^{-3/2}$) is obtained using a least-squares fit. (*b*) $W = 3.5$ mm, the dashed (respectively full) line represents the equation $Q = c_2 D$ where $c_2 = 0.58$ g s^{-1} mm^{-1} (respectively $c_2 = 0.43$ g s^{-1} mm^{-1}) is obtained using a least-squares fit.

h_p and the grain size d. Standard application of dimensional analysis or Π theorem gives us the relation between non-dimensional numbers (eight quantities, three units, which gives five non-dimensional numbers). The flux must scale like $\rho \ell^2 \sqrt{g\ell}$ where ℓ is any of D, W, h_p, d (and $\ell^2\sqrt{\ell}$ any combination of these lengths), and this flux must also be a function of the geometric ratios e.g. D/W, d/D, h_p/W, L/D (note that if we use the mass of grains in the silo, this will give us an extra parameter with dimension, which can be reduced to a new dimensional number, the packing fraction ϕ_b). Classical experiments on silos show that the flux is independent from the width L (if large enough), from the filling height h_p (if large enough) and from the grain size d (if small enough). We can therefore neglect the corresponding geometric ratios. This then reduces $Q/(\rho \ell^2 \sqrt{g\ell})$ (where ℓ is any of D, W) to a function of the aperture aspect ratio $\mathcal{A} = D/W$ only.

If W is large, the problem becomes bi-dimensional and D/W has no influence anymore. The velocity then scales like $\sqrt{gD}$, the size of the aperture being scaled by D, and the flux per transverse unit Q/W is $\rho D\sqrt{gD}$. This gives the equivalent for this rectangular geometry of the Hagen–Beverloo relation (Beverloo, Leniger & Van de Velde 1961; see a translation of the original article of Hagen in Tighe & Sperl 2007)

$$Q \propto W \rho \phi_b D \sqrt{gD}. \tag{3.1}$$

This scaling relation was recovered experimentally for a bottom aperture, spanning the width of a rectangular silo, by severals authors (Choi, Kudrolli & Bazant 2005; Benyamine *et al.* 2014). This behaviour is also observed in our experimental set-up with a side aperture. It can be seen in figure 4(*a*) where the flow rate is plotted as a function of the outlet length D for two particle diameters and for the larger silo thickness $W = 40$ mm. For a given particle diameter the data are well described by (3.1), see the full line and the dashed line in the figure. Therefore, following the Π theorem, the relevant normalisation for the flow rate seems to be $\rho\sqrt{gW^5}$, giving for the former relationship

$$\frac{Q}{\rho \phi_b \sqrt{gW^5}} = c_D \left(\frac{D}{W}\right)^{3/2}. \tag{3.2}$$

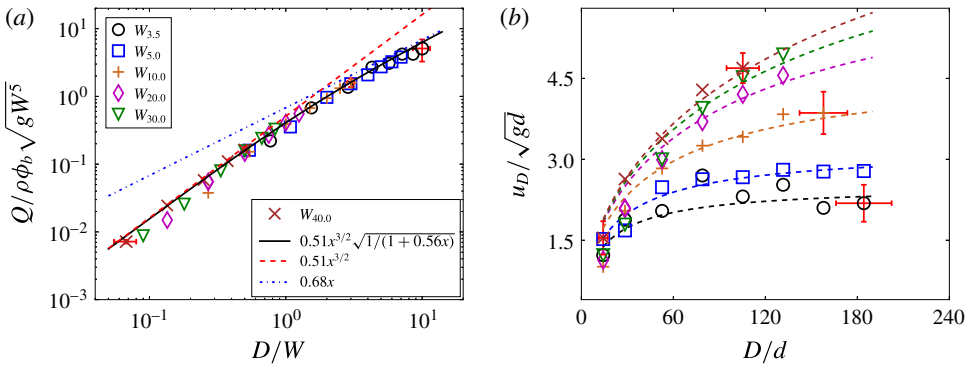

FIGURE 5. (Colour online) Experiments in the rectangular silo for a given particle diameter, $d = 190$ μm, and various silo widths, W. (a) Dimensionless mass flow rate $Q/(\rho\phi_b\sqrt{gW^5})$ as a function of D/W. The dashed line represents equation (3.2) with $c_D = 0.51$, the dashed-dotted line represents equation (3.3) with $c_W = 0.68$ and the solid line represents (3.4) with the same parameters. (b) Corresponding dimensionless discharge velocity $u_D/\sqrt{gd}$ as a function of D/d. The dashed lines represent equation (3.5) with the same parameters.

In the following section this scaling will be compared to the data obtained for the rectangular silo.

3.2. *Experimental results for the rectangular silo*

Figure 5(a) represents the dimensionless flow rate $Q_{\mathcal{A}} = Q/(\rho\phi_b\sqrt{gW^5})$ versus the aperture aspect ratio $\mathcal{A} = D/W$, for various thicknesses W and lengths D of the orifice and for a given diameter of particle $d = 190$ μm. In this representation the data collapse as suggested by the Π theorem.

As expected, for large thicknesses ($D/W \ll 1$), $Q_{\mathcal{A}}$ follows a power law with an exponent 3/2 corresponding to the Hagen–Beverloo relation (3.2), see the dashed line in the figure. However, for large values of D/W (i.e. thin enough silos), an important experimental result is that the dimensionless flow rate of particles depends linearly on the aperture aspect ratio (see the dashed-dotted line in figure 5a):

$$\frac{Q}{\rho\phi_b\sqrt{gW^5}} = c_W\frac{D}{W}. \tag{3.3}$$

This can also be seen in figure 4(b) where the flow rate is plotted versus the aperture length D for the smallest thickness explored $W = 3.5$ mm and for two particles diameters d. For a given particle diameter the flow rate indeed exhibits a linear trend $Q \propto D$. The transition between these two regimes occurs around a specific aperture ratio $\mathcal{A}_c \approx 2$. According to these two asymptotic regimes, we can thus propose a fitting formula for the flow rate:

$$\frac{Q}{\rho\phi_b\sqrt{gW^5}} = c_D\left(\frac{D}{W}\right)^{3/2}\frac{1}{\sqrt{1+(c_D/c_W)^2D/W}}. \tag{3.4}$$

As illustrated in figure 5(a) (solid lines), this formula describes well the flow rate dependency on aperture dimensions in any regime, with the fitting parameters $c_D = 0.51$ and $c_W = 0.68$.

These two regimes can be interpreted in term of the (horizontal) discharge velocity $u_D = Q/\rho\phi_b WD$, which can be expressed using (3.4) as

$$u_D = c_D\sqrt{gD}\frac{1}{\sqrt{1+(c_D/c_W)^2 D/W}}. \tag{3.5}$$

This relation again describes the data very well whatever the silo width as can be seen in figure 5(*b*) (dashed lines). The first regime corresponds to the classical Hagen–Beverloo relation with a velocity which scales with the aperture length:

$$(D/W) < \mathcal{A}_c, \quad u_D = c_D\sqrt{gD}. \tag{3.6}$$

Whereas in the second regime the discharge velocity scales with the aperture width:

$$(D/W) > \mathcal{A}_c, \quad u_D = c_W\sqrt{gW}. \tag{3.7}$$

This gives a velocity scaling with the smallest of the two lengths W and D.

Historically the Hagen–Beverloo relation was explained with the concept of a 'free-fall arch' located at the outlet, from which the particles fall freely. Several recent experiments and numerical simulations question this hypothesis. From an experimental point of view, Janda *et al.* (2012) and Rubio-Largo *et al.* (2015) showed that the granular medium remains dense, with a small dilation, close to the outlet and that the particles do not undergo a free fall. These observations were validated using discrete simulation (Rubio-Largo *et al.* 2015). Moreover Navier–Stokes simulations, assuming a continuum frictional rheology of the granular media, have been successfully used to recover the Hagen–Beverloo scaling as in Staron *et al.* (2012, 2014), Dunatunga & Kamrin (2015) and Davier & Bertails-Descoubes (2016), with very different numerical methods.

The fact that we recover the Hagen–Beverloo relation with a vertical aperture also tends to refute this concept, as pointed out by Sheldon & Durian (2010). Based on these observations, we performed a continuum simulation, using our Navier–Stokes solver with the granular rheology, to test whether we can reproduce at least qualitatively the experimental behaviour.

3.3. *Comparison with continuum numerical simulations*

We first performed continuum numerical simulations in the 2-D case. To compare with the experimental results we have plotted in figure 6(*a*) the dimensionless flow rate $Q_{\mathcal{A}} = Q/(\sqrt{gW^5})$ versus the aperture aspect ratio $\mathcal{A} = D/W$, using the same series of data but rescaled several times with each width W used for the pseudo-3-D simulations. In a pure bi-dimensional flow (red circles), the Navier–Stokes simulations recover the Hagen–Beverloo scaling, equation (3.2) (dashed line). This suggests that the $\mu(I)$ fluid rheology provides consistent results for the discharge of a silo with a side-located aperture.

Then, to mimic the effects of the lateral walls from a Hele-Shaw point of view, we added the friction term proportional to the pressure and aligned with the velocity, equation (2.4), and we varied the pseudo-width W (see the different symbols in figure 6*a*). We first notice that when the aperture ratio is small, similar to the experimental case, the data of the pseudo-3-D simulations are superimposed onto the 2-D simulations, and we recover the Hagen–Beverloo scaling, equation (3.2).

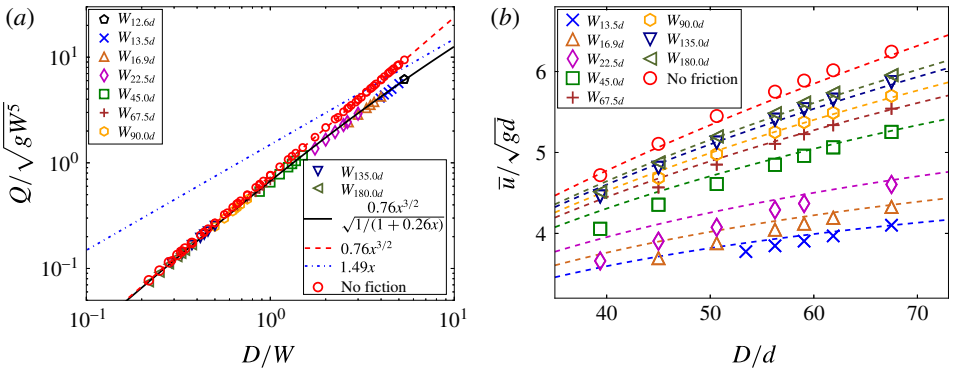

FIGURE 6. (Colour online) Continuum simulations results in two dimensions and in pseudo three dimensions for various W with $H = 360d$, $L = 90d$ and $D = 45d$. (*a*) Flow rate Q normalised by $\sqrt{gW^5}$ as a function of D/W. The dashed line represents equation (3.2) with $c_D = 0.76$, the dashed-dotted line represents equation (3.3), with $c_W = 1.49$, and the solid line represents equation (3.4), with the same parameters. (*b*) Mean horizontal velocity at the orifice $\overline{u}/\sqrt{gd}$, as a function of D/d. The dashed lines represent equation (3.5), with the same parameters.

When increasing the aperture ratio, we observe a departure from this scaling towards a regime where $Q_{\mathcal{A}} \propto \mathcal{A}$ (see the dashed-dotted line). We can see that we do not completely reach this regime due to the numerical upper limit of achievable values for f_w, however the data are well described by (3.4) with $c_D = 0.76$ and $c_W = 1.49$ (solid line).

Following the experimental section, the dimensionless mean horizontal velocity at the outlet, $\overline{u}/\sqrt{gd}$, is plotted versus the dimensionless outlet length D/d in figure 6(*b*). We observe the same trends as for the experimental data: in the regime controlled by the outlet length D, the velocity tends toward the Hagen–Beverloo scaling ((3.6) and 2-D data) whereas when the ratio $\mathcal{A}$ increases, the velocity tends toward the regime controlled by the silo width given by (3.7). Again each series of data for a given W are fairly well described by (3.5) (dashed lines).

In the continuum simulation, the width of the silo appears only in the term describing the side wall friction, which suggests that the second regime is controlled by this term. It is interesting to note that in the regime dominated by the lateral friction the flow rate per unit length at a given D is lower than in the first regime. Even if we cannot fully reach the second regime ($\mathcal{A} \gg 1$), we carry on with the analysis and present some comparisons of the details of the internal fields at the limit of the numerical model.

Figure 7 shows the velocity field and the streamlines of both the experimental and the numerical runs for increasing silo width. The numerical velocity field (figure 7*b*) is qualitatively very similar to the experimental velocity field (figure 7*a*). In both configurations, the streamlines tend to vertical lines upward from the orifice at a distance which decreases when W increases. On the same figures, we observe that the flowing zone is found to be thinner when the lateral friction increases (i.e. when W decreases). The limit of the stagnant zone for various outlet sizes D is plotted in figure 8 both for the experiment (*a*), and the continuum simulation (*b*), in the regime dominated by the lateral friction. Interestingly this position does not depend on D in either cases, but depends strongly on W.

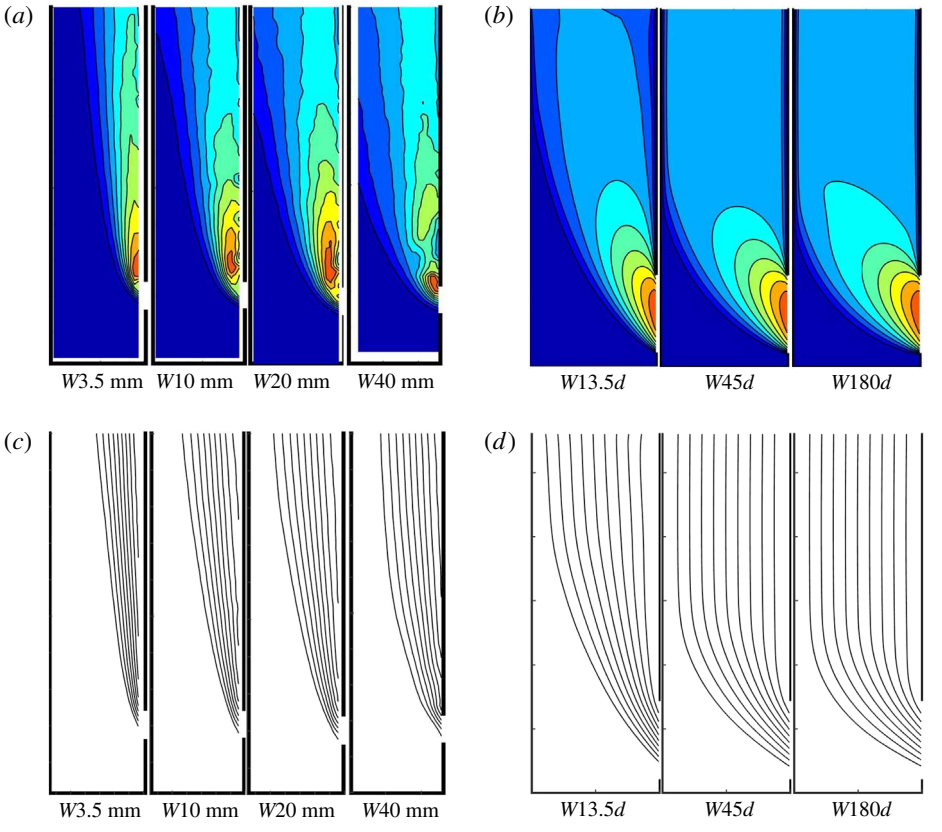

FIGURE 7. (Colour online) Velocity field (*a*,*b*) and streamlines (*c*,*d*) for the experiment (*a*,*c*) with $D = 20$ mm, $d = 1129$ μm and $W = [3.5, 10, 20, 40]$ mm, and for the continuum simulation (*b*,*d*) with $D = 56.25d$ and $W = [13.5d, 45d, 180d]$.

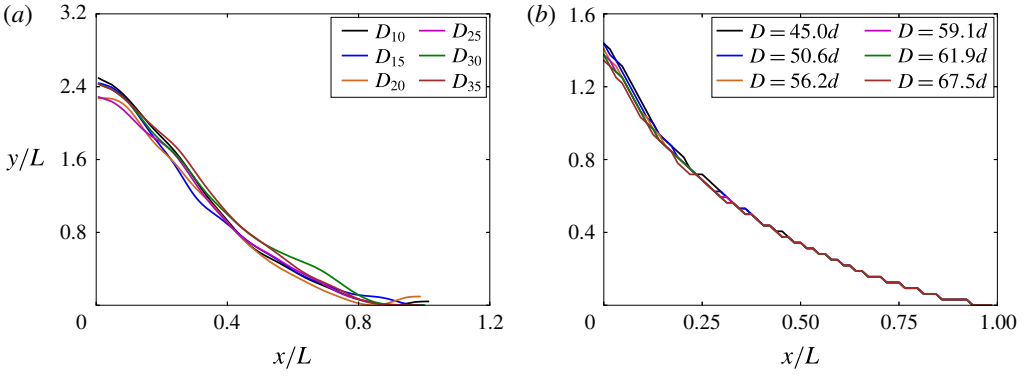

FIGURE 8. (Colour online) Limit of the stagnant zone for various D: (*a*) experiments with $W = 5$ mm and (*b*) continuum simulations with $W = 17.4d$.

We may explain these behaviours at small W by looking at the Navier–Stokes equations. Let us consider a steady flow (implying that we neglect inertia). As the

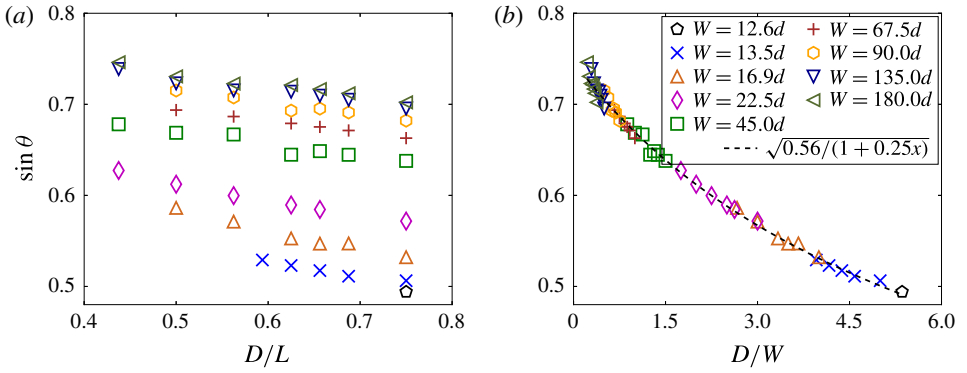

FIGURE 9. (Colour online) Continuum simulation results: angle of inclination θ of the central streamline at the orifice relative to vertical for various W (a) versus D/L, (b) versus D/W. The dashed line represents equation (3.11) with $\gamma_1 = 0.56$ and $\gamma_2 = 0.25$.

friction at the walls increases when W decreases, the friction term (of magnitude $\mu_w p/W$) will be at most as large as gravity (ρg). The gradients of the stress tensor are of order $\mu_s p/L$. This order of magnitude may be rewritten as $(\mu_s/\mu_w)(W/L)\mu_w p/W$. It is clearly smaller than $\mu_w p/W$ as $(\mu_s/\mu_w) = O(1)$ and $(W/L) \ll 1$. Hence, as the wall friction increases to balance gravity, the momentum equation can be approximated as:

$$0 \simeq \frac{2\mu_w p}{W} O\left(\frac{\mu_s W}{\mu_w L}\right) \boldsymbol{e} + \rho \boldsymbol{g} - \frac{2\mu_w p}{W} \frac{\boldsymbol{u}}{|\boldsymbol{u}|}, \tag{3.8}$$

where $\boldsymbol{e}$ is a unit vector in the main direction of the force resulting from internal friction. The velocity $\boldsymbol{u}$ is aligned with gravity at first order, the more so as the thickness decreases. This is noticeable in figure 7(*c*,*d*) where for small W the streamlines are clearly more vertical than for larger W. To quantify this effect, we have plotted the angle of inclination θ of the central streamline at the orifice relative to the vertical in figure 9. If we note u_0 the horizontal velocity at the centre of the outlet and U_0 the norm of the velocity at this position, we can write $\sin\theta = u_0/U_0$ (note that u_0 is proportional to the previously defined discharge velocity u_D, as we will see in § A.2). We observe in figure 9(*a*) that this angle decreases slightly with D and strongly with W as expected. More interestingly, if plotted versus D/W (figure 9*b*), the data superimpose. In order to study the scaling relation of $\sin\theta$, we then turn to the dependency of the norm of the velocity U_0 and horizontal velocity u_0 on W and D. In figure 10 we have represented the norm of the velocity $U_0/\sqrt{gd}$ on the central streamline at the orifice versus D/d for various W. Surprisingly we can see that the norm of the velocity does not significantly depend on W. The data can be described by

$$U_0 = c_U \sqrt{gD}, \tag{3.9}$$

with $c_U = 1.2$. This suggests that the kinetic energy always scales like $\rho g D$ whatever the lateral friction. For the horizontal velocity u_0, since the flow rate $Q \propto u_0 W D$, from (3.4), we can write

$$u_0 \propto \sqrt{gD} \sqrt{\frac{1}{1 + (c_D/c_W)^2 D/W}}. \tag{3.10}$$

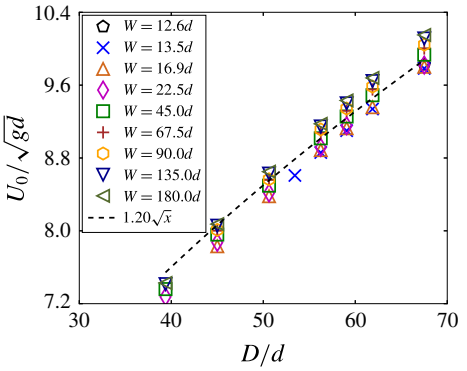

FIGURE 10. (Colour online) Continuum simulation results: norm of the velocity $U_0/\sqrt{gd}$ on the central streamline at the orifice versus D/d for various W. The dashed line represents equation (3.9) with $c_U = 1.2$.

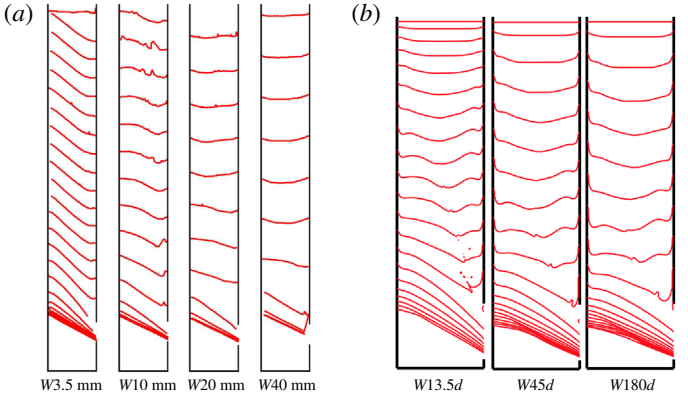

FIGURE 11. (Colour online) Profiles of the top surface of granular materials for various W at constant time steps: (*a*) experiments with $D = 25$ mm, $d = 190$ μm, time interval $\Delta t_e = 0.5$ s, (*b*) continuum simulation with $D = 56.25d$ and time interval $\Delta t_s/\sqrt{d/g} = 9.5$.

We can thus obtain

$$\sin\theta = \sqrt{\frac{\gamma_1}{1+\gamma_2 D/W}}. \tag{3.11}$$

Moreover we see that the data in figure 9(*b*) are well described by this formulation with $\gamma_1 = 0.56$ and $\gamma_2 = 0.25$, with the fitting parameter $\gamma_2 = 0.25$ corresponding to $(c_D/c_W)^2 = 0.26$.

Finally figure 11 shows the time evolution of the top surface of granular material for various silo widths for (*a*) the experiment and (*b*) the continuum simulation. From experiments we can see that the surface of particles begins to tilt in the early stage for a small width W, whereas it remains constant till the last stage for the largest W. The tilted interface exhibits a slope starting from the wall opposite to the outlet and reaches a flattened surface, or sometimes even a small bump, on the wall containing the outlet. The slope of the interface is higher than the angle of repose for $W = 3.5$ mm, and smaller than the angle of repose for $W = 10$ mm.

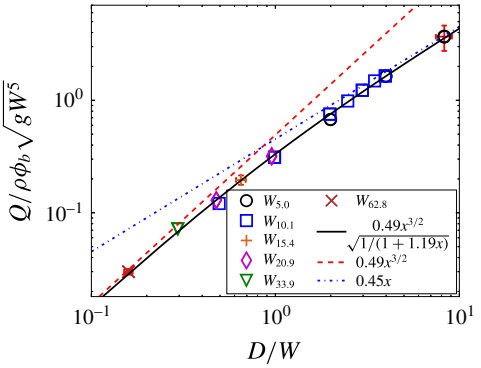

FIGURE 12. (Colour online) Experimental results in the cylindrical silo: dimensionless mass flow rate $Q/(\rho\phi_b\sqrt{gW^5})$ as a function of the aperture aspect ratio D/W. The dashed line represents equation (3.2) with $c_D = 0.49$, and the dashed-dotted line represents equation (3.3) with $c_W = 0.46$.

In continuum simulations, we explored a smaller range of W, the smallest W case $W = 13.5d$, is comparable to the case $W = 20$ mm in the experiments, but we clearly recover the same trend: the larger the thickness W, the longer the interface remains symmetrical. Note also that the no-slip conditions imposed at the wall are not exactly the same as in the experiments, where a sliding velocity is observed. Nevertheless, the same qualitative profiles are obtained. This behaviour is consistent with the previous observation: for large W, the flow far from the outlet is symmetrical. For small W, the lateral friction breaks this symmetry and localises the flow on the side of the outlet, which inclines the surface in this direction.

3.4. *Experimental results in the cylindrical silo*

The previous results were given for a simplified geometry, with a rectangular silo and an outlet which spans the width of the silo. Experimentally we also performed measurements of the flow rate for a cylindrical silo, with an outlet located at its side as schematised in figure 1(*b*). This situation generates a flow in a fully 3-D geometry, and is of practical interest. To characterise the different roles played by the length D and the width W of the outlet, we have plotted in figure 12 the dimensionless mass flow rate $Q/(\rho\phi_b\sqrt{gW^5})$ as a function of the aperture aspect ratio D/W, as done in the rectangular configuration.

As suggested by the Π theorem in § 3.1 the data superimpose in this representation. Moreover, we observe the same behaviours as in rectangular silos. For large W, the flow rate follows the Hagen–Beverloo relation ((3.2), dashed line in the figure) and for small W, the flow rate follows (3.3) (dashed-dotted line in the figure) suggesting that the flow is dominated by the lateral friction. Over the whole range, the data are well correlated by (3.4) (solid line in the figure) with $c_D = 0.49$ and $c_W = 0.46$. The fitting parameter c_w is found to be slightly smaller than that in the rectangular silo. This suggests that the dissipation is higher in the cylinder, and more specifically in the regime controlled by the lateral friction where we can assume that the friction with a smooth lateral wall is smaller than that with an erodible granular media. Consequently, the transition between the two regimes occurs for a smaller aperture aspect ratio $\mathcal{A}_c \approx 1$.

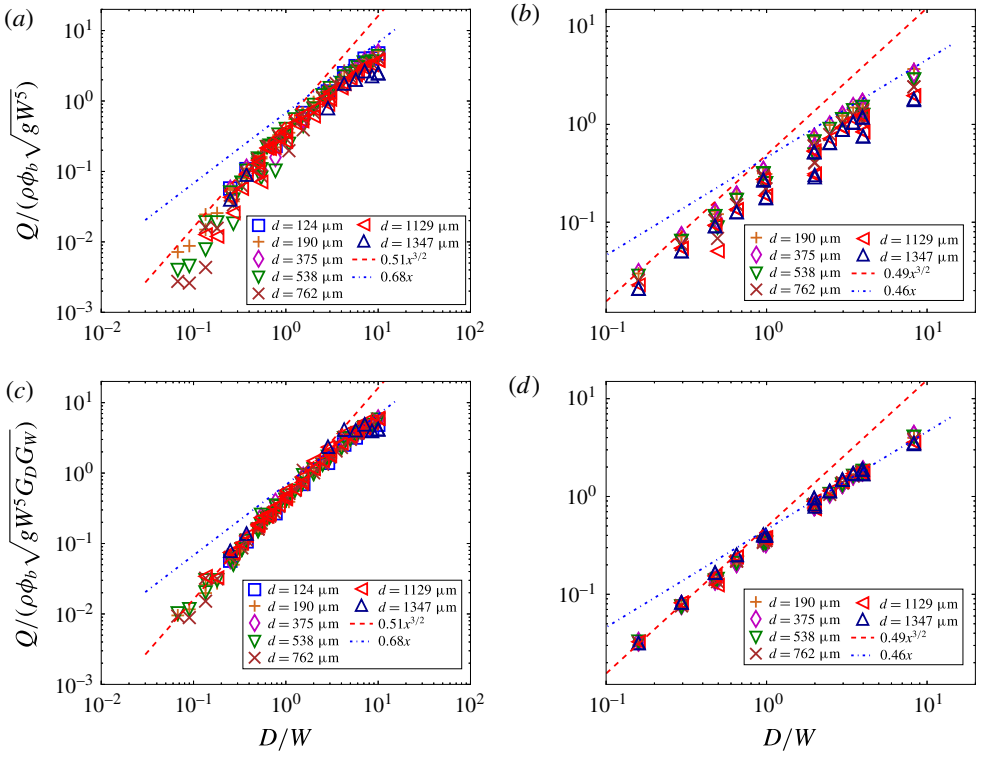

FIGURE 13. (Colour online) Mass flow rate Q as a function of D/W for various d for (a,c) rectangular silos and (b,d) cylindrical silos, normalised in (a,b) by $(\rho\phi_b\sqrt{gW^5})$ and in (c,d) by $\rho\phi_b\sqrt{gW^5}G_D(D/d)G_W(W/d)$ (see (3.12)) with the fitting parameters $\beta_D = \beta_W = 0.1$, $\alpha_D = 1$ and $\alpha_W = 0.46$ (see appendix A). The dashed and dashed-dotted lines are the same as in figures 5 and 12.

3.5. *Dependency of the flow rate on the particle diameter*

The previous results are shown for a given small particle diameter $d = 190$ µm. In this section we focus on the influence of the particle diameter. We have shown that the flow rate of discharge of a silo with a lateral outlet depends on the aperture aspect ratio $\mathcal{A} = D/W$, and exhibits two regimes of flow described by (3.2) for small $\mathcal{A}$ and by (3.3) for large $\mathcal{A}$. When the particle diameter is varied, these scaling relations seem to remain valid, as can been seen in figure 4(a,b) where the flow rate is plotted versus D for two particle diameters, $d = 190$ µm and $d = 1129$ µm, in the two regimes. In each regime the same scaling is found for the two grain sizes, however we observe a shift of these relations towards smaller flow rates when the particle diameter increases. This behaviour can be seen in figure 13(a,c) where the dimensionless flow rate $Q_{\mathcal{A}} = Q/\rho\phi_b\sqrt{gW^5}$ is plotted as a function of D/W for both the rectangular silos and the cylindrical silo for all the batch of particles we used. The two regimes are recovered whatever the particle diameter, see the dashed line and the dashed-dotted line. However there is a significant scattering of the data above the relation fitted for the smallest particle size $d = 190$ µm.

To model the dependency of the flow rate on the particle diameter, we follow the work of Janda *et al.* (2012). In this framework we suppose that the particle size has

to be accounted for through the number of beads in the aperture via a geometrical function, significant when this number is small. We take the two dimensions of the aperture into account and thus we suppose that the flow rate depends on two geometrical functions based on the number of beads in the aperture length D/d and in the aperture width W/d. The details of this approach and its validation using a 2-D discrete numerical simulation are given in the appendix. This yields the following expression for the flow rate:

$$Q = C_l' \rho \phi_b G_D \left(\frac{D}{d}\right) G_W \left(\frac{W}{d}\right) F \left(\frac{D}{W}\right) WD\sqrt{gD}, \tag{3.12}$$

with $G_D(D/d) = [1 - \alpha_D \mathrm{e}^{-\beta_D(D/d)}]$, $G_W(W/d) = [1 - \alpha_W \mathrm{e}^{-\beta_W(W/d)}]$ and $F(D/W) = \sqrt{1/[1 + \gamma_2 D/W]}$.

Figure 13 shows the normalised flow rate using the geometrical functions, $Q/[\rho\phi_b G_D(D/d) G_W(W/d)\sqrt{gW^5}]$, as a function of the aperture aspect ratio D/W for the whole range of particle diameters for (*c*) rectangular silos and (*d*) cylindrical silos. In this representation the data collapse and can be well adjusted by the same asymptotic relations in two regimes as in figures 5 and 12.

We propose additional analysis in the appendix. The 2-D discrete numerical simulation shows that the velocity at the outlet may follow the same geometrical relation than the volume fraction. As the continuum simulation described correctly most of the observations on the discharge of a silo with a lateral aperture for a given particle diameter we wonder if the continuum simulation is able to recover partially the dependency on the particle size of the flow rate. Indeed, the $\mu(I)$ rheology contains the information on the particle diameter in the definition of the inertial number $I = d\sqrt{2}D_2/(\sqrt{p/\rho})$. Even though a dependency on the particle diameter is observed in the 2-D case, the profiles present a larger asymmetry than the one predicted by the 2-D discrete simulations. This can be due to the fact that the volume fraction has been assumed to be uniform, whereas the complete $\mu(I)$-rheology, that includes a $\phi(I)$ relation, would predict a dilation of the granular medium when it is sheared.

4. Conclusion and perspectives

Using experiments, 2-D discrete simulations and continuum simulations we have studied the discharge of a silo with a lateral orifice. Experimentally we have observed two regimes of flow, either in a rectangular silo with an orifice spanning the thickness W of the silo or in a cylindrical silo. The first regime, observed for small aperture aspect ratios $\mathcal{A} = D/W$, corresponds to the well-known Hagen–Beverloo regime with a flow rate $Q \propto WD^{3/2}$. The second regime, observed for large aperture aspect ratios $\mathcal{A} > \mathcal{A}_c$, follows $Q \propto W^{3/2}D$. We have proposed an empirical relation which predicts the flow rate depending on the aperture dimensions and which recovers both regimes. The continuum simulation, using the frictional $\mu(I)$ rheology and solved in two dimensions with an additional force to take into account the wall friction in a Hele-Shaw spirit, is found to describe qualitatively these two regimes and most of the internal details of the flow field observed experimentally in the rectangular silo, notably the fact that the velocity field is aligned with gravity when lateral wall friction is large. The dependency on the silo width suggests that the large $\mathcal{A}$ regime is dominated by the lateral friction, and it seems reasonable to think that the small $\mathcal{A}$ regime is controlled by the internal friction.

We have found that the particle diameter matters only when the number of beads through the smallest orifice dimension is sufficiently small. The flow rate dependency on this parameter can be reasonably described using two geometrical functions $G_\ell(\ell/d) = 1 - \alpha e^{-\beta \ell/d}$ based respectively on W and on D. A large part of this behaviour is well reproduced using 2-D discrete simulations. Interestingly a dependency on the particle diameter is also observed in the 2-D continuum simulation but it predicts different velocity profiles which can be due to the fact that in the continuum simulation the volume fraction does not vary.

In future work these promising observations need to be confirmed by conducting systematic 3-D simulations. Preliminary 3-D continuum simulation results indicate that the Hagen–Beverloo relation is obtained for a silo with bottom aperture. Extra developments have to be done to include realistic boundary conditions to represent particle–wall friction as well as the volume fraction variation $\phi(I)$.

Acknowledgements

We would like to thank P. Cervetti, S. Noel and F. Ratouchniak for technical assistance. This work has been carried out in the framework of the Labex MEC (ANR-10-LABX-0092) and of the A*MIDEX project (ANR-11-IDEX-0001-02), funded by the 'Investissements d'Avenir' French Government program managed by the French National Research Agency (ANR).

Supplementary material

Supplementary material is available at https://doi.org/10.1017/jfm.2017.543.

Appendix A. Additional analysis

In this section we focus on the influence of the particle diameter. We first present an analysis of the experimental results based on the work of Janda *et al.* (2012). We then discuss the role of the particle diameter on the flow close to the outlet using 2-D contact dynamics simulations. Finally, we compare these results to the continuum numerical simulations.

A.1. *Experimental results and discussion*

To take the dependency on the particle diameter into account, as observed in figure 13(*a*,*b*), we suppose that the observations made experimentally by Janda *et al.* (2012), and numerically by Zhou *et al.* (2015) for a two-dimensional silo with an orifice placed at the bottom of the silo remain valid in our geometry. We make the following assumptions:

(i) We suppose that the horizontal velocity profile together with the density profile at the outlet are self-similar when varying the length of the hole $R = D/2$. The flow rate is then given by

$$Q = \rho W \int\!\!\int_{-R}^{R} \phi(y) u(y)\, \mathrm{d}y = c \rho W D \bar{\phi} \bar{u}, \tag{A 1}$$

where c is a constant of integration and $\bar{\phi}$ and $\bar{u}$ represent the mean density and the mean horizontal velocity at the outlet respectively. The flow rate is then determined by these two quantities.

(ii) Following (3.5), the mean horizontal velocity tends asymptotically as d decreases towards

$$\xi_v\sqrt{gD}\sqrt{\frac{1}{1+\gamma_2 D/W}}=\xi_v\sqrt{gD}F(D/W), \tag{A 2}$$

where $F(D/W)=\sqrt{1/[1+\gamma_2 D/W]}$, which corresponds to the value for infinitely small particles.

(iii) The granular medium tends to dilate at the outlet to maintain the flow. However for a large number of beads in the aperture, we suppose that it tends towards a fraction of the bulk density asymptotically, $\xi_\phi\phi_b$, with ξ_ϕ a constant.

(iv) We suppose that both the mean density and the mean velocity depend on the number of beads in the aperture via a geometrical function. To take the two dimensions of the aperture into account, we suppose that the flow rate depends on two geometrical functions based on the number of beads in the aperture length D/d, and in the aperture width W/d. We assume that this geometrical function can be fitted by an exponential saturation

$$Q=C_l'\rho\phi_b G_D\left(\frac{D}{d}\right)G_W\left(\frac{W}{d}\right)F\left(\frac{D}{W}\right)WD\sqrt{gD}, \tag{A 3}$$

with $G_D(D/d)=[1-\alpha_D \mathrm{e}^{-\beta_D(D/d)}]$ and $G_W(W/d)=[1-\alpha_W \mathrm{e}^{-\beta_W(W/d)}]$.

To test these hypotheses, we isolated each geometrical function by plotting the dimensionless flow rate $Q/(\rho\phi_b WDF(D/W)\sqrt{gD})$ as a function of the number of beads in the typical length ℓ/d for the two regimes (i) $\ell=D$ and (ii) $\ell=W$. In figure 14(*a*,*c*) all the data for the rectangular silo are plotted and no clear trend can be observed. However, when considering each regime separately, as done in figure 14(*b*,*d*), i.e. by selecting the experiments corresponding to the first regime $\ell=D$ (and the second regime $\ell=W$), taking $D<1.8W$ (respectively $D>2.2W$), and considering a large number of beads in the second direction of the orifice $W>10d$ (respectively $D>20d$), the remaining data superimpose and can be well adjusted by an exponential saturation with the fitting parameters $\alpha_D=1$, $\beta_D=0.1$, $\alpha_W=0.46$ and $\beta_W=0.1$ (see the black lines in the figures). These parameters are of the same order of magnitude as that of the literature for both geometrical functions. It is interesting to note that the same β is recovered in the two directions. The same procedure has been followed for the cylindrical silo. Again, we find that both geometrical functions can be well adjusted by an exponential saturation, with the fitting parameters $\alpha_D=0.59$, $\beta_D=0.08$, $\alpha_W=0.61$, and $\beta_W=0.08$, in agreement with the literature.

As shown in figure 13(*c*,*d*) it seems that the geometrical functions built on the two dimensions of the aperture correctly describe the dependency of the flow rate on the particle diameter. To further test some of the assumptions, we performed a 2-D discrete simulation of the discharge flow of a silo from a lateral orifice that allows to study the effective velocity and volume fraction profiles.

A.2. *Discrete simulations in two dimensions*

Discrete particle simulations are described in § 2.2. In this two-dimensional configuration, following the same methodology as for the bottom orifice done experimentally by Janda *et al.* (2012) and with a 2-D discrete simulation by Zhou

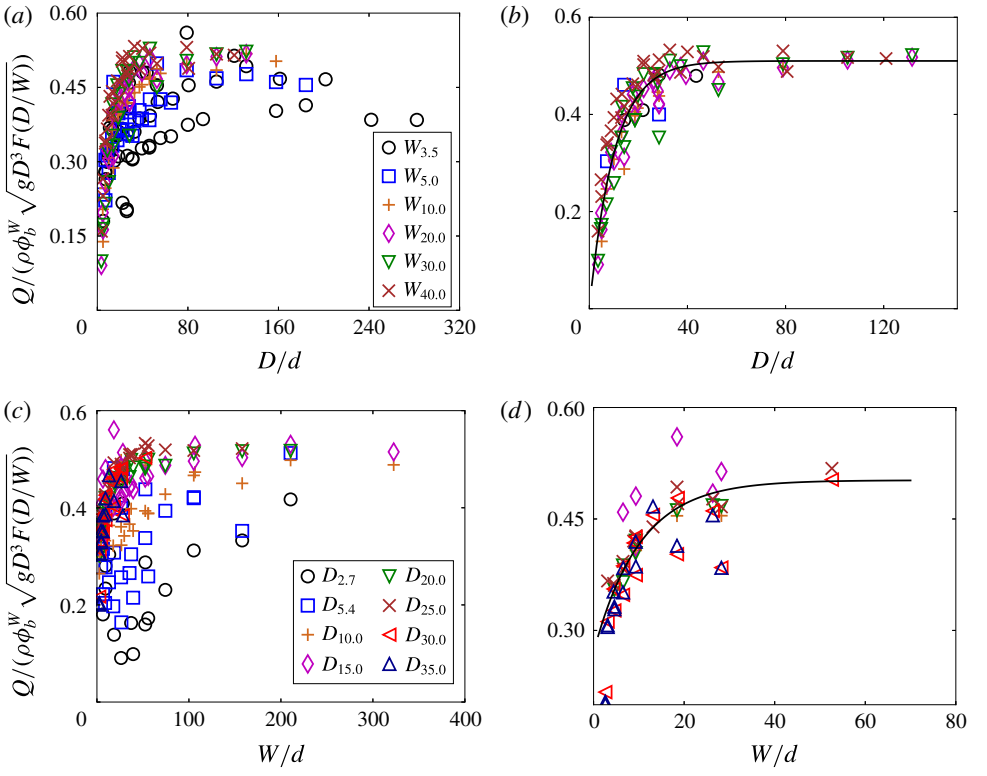

FIGURE 14. (Colour online) Experimental results obtained with rectangular silos: dimensionless flow rate $Q/(\rho\phi_b WDF(D/W)\sqrt{gD})$ versus (a,b) D/d and (c,d) W/d. Selected experimental runs: (a,c) all the runs, (b) $D < 1.8W$ and $W > 10d$, (d) $D > 2.2W$ and $D > 20d$. The full lines represent the geometrical functions $G_D(D/d) = [1 - \alpha_D e^{-\beta_D(D/d)}]$ and $G_W(W/d) = [1 - \alpha_W e^{-\beta_W(W/d)}]$ with $\alpha_D = 1$, $\beta_D = 0.1$, $\alpha_W = 0.46$ and $\beta_W = 0.1$ respectively.

et al. (2015), we are able to test most of the hypotheses (i) to (iv) made in the previous section for the Hagen–Beverloo regime.

(i) We have first assumed that at the lateral outlet, the horizontal velocity profile together with the density profile are self-similar when varying the length of the hole $R = D/2$. Figure 15$(a$–$c)$ shows the vertical profile of the volume fraction, ϕ, of the horizontal velocity, u, and of the vertical velocity, v, for various aperture lengths, D, for a given particle diameter $d = 2$ mm. The vertical axis, y, is oriented upward and its origin is located at the middle of the outlet. Similar to the case of an aperture placed at the bottom of the silo, the volume fraction profile is found to be self-similar when normalised by the mean volume fraction, $\bar{\phi}$ as shown in figure 15(d). The self-similar profile is slightly dissymmetrical, the top of the profile exhibiting a slightly higher dilatancy at the edge than at the bottom. Nevertheless, it can be well fitted by

$$\phi(y) = \bar{\phi}\gamma(\nu_\phi)\left[1 - \left(\frac{y}{R}\right)^2\right]^{\nu_\phi}, \tag{A 4}$$

where $\gamma(\nu) = (2/\sqrt{\pi})\Gamma(\nu + 3/2)/\Gamma(\nu + 1)$. The fitting parameter, $\nu_\phi = 0.21 \pm 0.01$, obtained using the least squares method, is similar to that obtained for a bottom

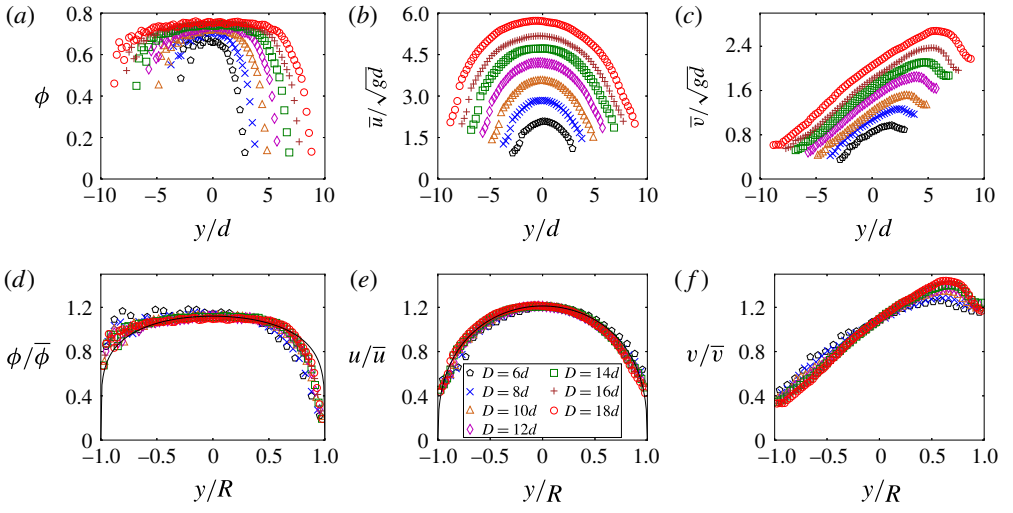

FIGURE 15. (Colour online) (*a–f*) Flow of particles of diameter of $d = 2$ mm for different outlet diameters. Vertical profiles of (*a*) the volume fraction, ϕ, (*b*) the horizontal velocity, u, and (*c*) the vertical velocity, v, versus the vertical position, y. Vertical profiles of (*d*) the volume fraction normalised by the mean volume fraction, $\bar{\phi}$, (*e*) the horizontal velocity made dimensionless by the mean horizontal velocity, $\bar{u}$, and (*f*) the vertical velocity made dimensionless by the mean vertical velocity, $\bar{v}$, versus the position normalised by the outlet radius ($R = D/2$). The full lines represent in (*d*) equation (A 4) with $\nu_\phi = 0.21$ and in (*e*) equation (A 5) with $\nu_v = 0.38$ respectively.

aperture $\nu_\phi = 0.19 \pm 0.01$ by Zhou *et al.* (2015). In the same way, once normalised by the mean horizontal velocity, $\bar{u}$, the horizontal velocity profile is found to be self-similar and well adjusted by

$$u(y) = \bar{u}\gamma(\nu_v)\left[1 - \left(\frac{y}{R}\right)^2\right]^{\nu_v}, \tag{A 5}$$

with the fitting parameter, $\nu_v = 0.38 \pm 0.01$ obtained using the least-squares method. This parameter is identical to that obtained for the vertical velocity by Zhou *et al.* (2015) in the silo with a bottom aperture. Finally, the horizontal velocity profile is also found to be self-similar. The self-similar profile is clearly non-symmetric, exhibiting mainly a linear profile on the main part of outlet with a maximum close to the top where the velocity decreases toward the edge. The first hypothesis is hence fulfilled and the flow rate is given by $Q = c\rho D\bar{\phi}\bar{u}$, where c is a constant.

To test the hypotheses (ii)–(iv), we plotted the mean volume fraction, $\bar{\phi}$ and the mean horizontal and vertical velocities, $\bar{u}$ and $\bar{v}$, as a function of the aperture length, D, for two particles diameters, $d = 2$ mm (○) and $d = 6$ mm (△), as seen in figure 16 (*a–c*). Clearly, all the variables depend on the particle diameters. In figure 16(*d–f*), the same variables are plotted, normalised by the assumed asymptotic behaviour, as a function of the number of beads in the aperture. The data collapse on single curves, as observed for the silo with a bottom aperture, which are well adjusted by an exponential saturation as expected,

$$\bar{\phi} = \xi_\phi\phi_b\left[1 - \alpha_\phi e^{-\beta(D/d)}\right] = \xi_\phi\phi_b G_\phi\left(\frac{D}{d}\right), \tag{A 6}$$

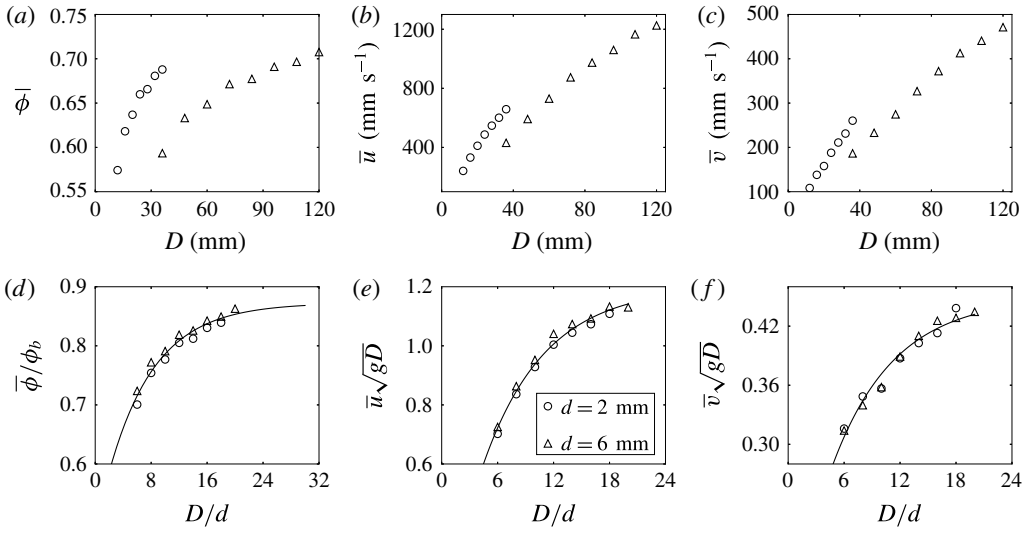

FIGURE 16. (*a*) Mean volume fraction at the outlet, $\bar{\phi}$, (*b*) mean horizontal velocity, $\bar{u}$, and (*c*) mean vertical velocity, $\bar{v}$, versus the diameter apertures D, for two particle diameters. (*d*) Mean volume fraction at the outlet, $\bar{\phi}$, normalised by the bulk volume fraction, ϕ_b, (*e*) mean horizontal velocity, $\bar{u}$, made dimensionless by $\sqrt{gd}$ and (*f*) mean vertical velocity, $\bar{v}$, made dimensionless by $\sqrt{gd}$, versus the number of beads in the apertures D/d, for two particle diameters. The full line represent in (*d*) equation (A 6) with $\xi_\phi = 0.87$, $\alpha_\phi = 0.44$ and $\beta = 0.15$, in (*e*) equation (A 7) with $\xi_u = 1.2$, $\alpha_u = 0.98$ and $\beta = 0.15$ and in (*f*) equation (A 8) with $\xi_v = 0.45$, $\alpha_v = 0.78$ and $\beta = 0.15$, respectively.

$$\bar{u} = \xi_u \sqrt{gD}\left[1 - \alpha_u \mathrm{e}^{-\beta(D/d)}\right] = \xi_u \sqrt{gD} G_u\left(\frac{D}{d}\right), \tag{A 7}$$

$$\bar{v} = \xi_v \sqrt{gD}\left[1 - \alpha_v \mathrm{e}^{-\beta(D/d)}\right] = \xi_v \sqrt{gD} G_v\left(\frac{D}{d}\right), \tag{A 8}$$

with the fitting parameters $\beta = 0.15$, $\xi_\phi = 0.87$, $\alpha_\phi = 0.44$, $\xi_u = 1.2$, $\alpha_u = 0.98$, $\xi_v = 0.45$, $\alpha_v = 0.78$, obtained using the least-squares method. Once again, these parameters closely match those obtained by Zhou *et al.* (2015) for the bottom configuration. The same β, fitted on the volume fraction, is found to correctly adjust the mean velocity variations. This suggests that the same phenomenon is involved in the variation at the outlet of the volume fraction and of the velocities with respect to the particle size. These equations also suggest that in the Hagen–Beverloo regime, the angle of inclination of the streamline at the outlet, defined as $\tan(\theta) = \bar{u}/\bar{v}$ has low dependency on the outlet size D through a geometrical function G_u/G_v. Finally the flow rate is given by

$$Q = C_l' \rho \phi_b \sqrt{gD} G_\phi\left(\frac{D}{d}\right) G_u\left(\frac{D}{d}\right) \approx C_l' \rho \phi_b \sqrt{gD} G\left(\frac{D}{d}\right), \tag{A 9}$$

where $C_l' = \xi_\phi \xi_v \gamma(\nu_v)\gamma(\nu_\phi) \int_0^1 (1 - t^2)\,\mathrm{d}t = 1.08$ and $G = [1 - \alpha \mathrm{e}^{-\beta(D/d)}]$ with $\alpha = \alpha_\phi + \alpha_u$. In the range of number of beads in the aperture ($D/d > 6$), the approximation of $G \approx G_u G_\phi$ leads to less than 5 % of error. This equation adjusts the data well with the

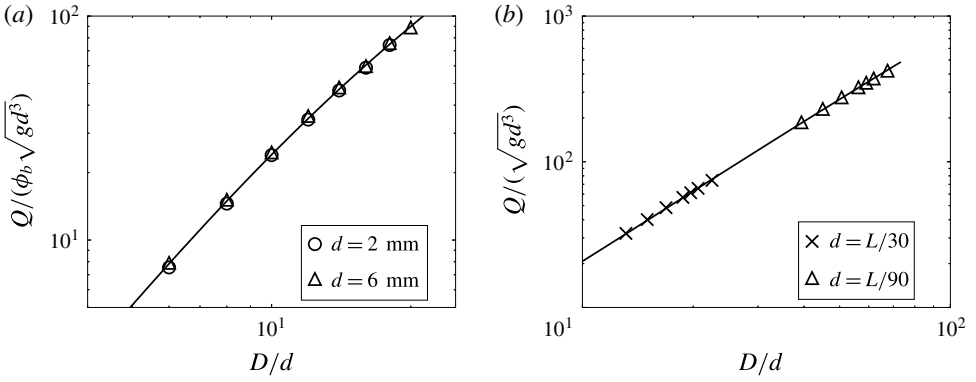

FIGURE 17. Flow rate made dimensionless by $\sqrt{gd^3}$ versus the number of beads in the aperture D/d for the 2-D case, (*a*) discrete simulation, (*b*) continuum simulation. The full lines represent equation (A 9) with (*a*) $C_l' = 1.08$ and (*b*) $C_l' = 0.78$.

fitting parameter $C_l' = 1.08$, as seen in figure 17, and is similar to (A 3) considering $W = \infty$.

Using 2-D discrete simulations we have shown that the dependence of the flow rate on the particle size can be modelled using a geometrical function which depends only on the number of beads in the aperture. This geometrical function is seen to influence both the volume fraction at the outlet, bigger particles leading to a dilation, and the velocity, bigger particles leading to slower flow. It would be interesting in future work to conduct 3-D discrete simulations to see if we recover the same geometrical function for the number of beads in the silo width, in the regime dominated by the lateral friction, as suggested by the experimental results.

A.3. *Continuum simulation*

We have seen in § 3 that the continuum simulation described correctly most of the observations on the discharge of a silo with a lateral aperture, for various D and various W but for a given particle diameter. However the $\mu(I)$ rheology contains the information on the particle diameter in the definition of the inertial number $I = d\sqrt{2}D_2/(\sqrt{p/\rho})$. In this section we wonder if the continuum simulation is able to recover partially the dependency on the particle size of the flow rate. Indeed, even if this simulation considers a constant volume fraction, the 2-D discrete simulations have shown that the velocity at the outlet may follow the same geometrical relation than the volume fraction.

Figure 18 presents the vertical profile at the outlet of the horizontal velocity, the vertical velocity and the norm of the velocity, for a given particle diameter in the 2-D case. Interestingly, when normalised by the mean value, these profiles are again found to be self-similar. However, contrary to the discrete simulations, the horizontal velocity profile exhibits a strong asymmetry between the top and the bottom of the outlet. As a consequence, the adjustment by the (A 5) with the fitting parameter $\nu_u = 0.31 \pm 0.01$ obtained using least-squares method is not satisfactory. However the vertical velocity profile resembles the discrete simulation result. Interestingly, the profile of the norm of the velocity is found to remain symmetrical and is well adjusted by (A 5) with $\nu_v = 0.31$.

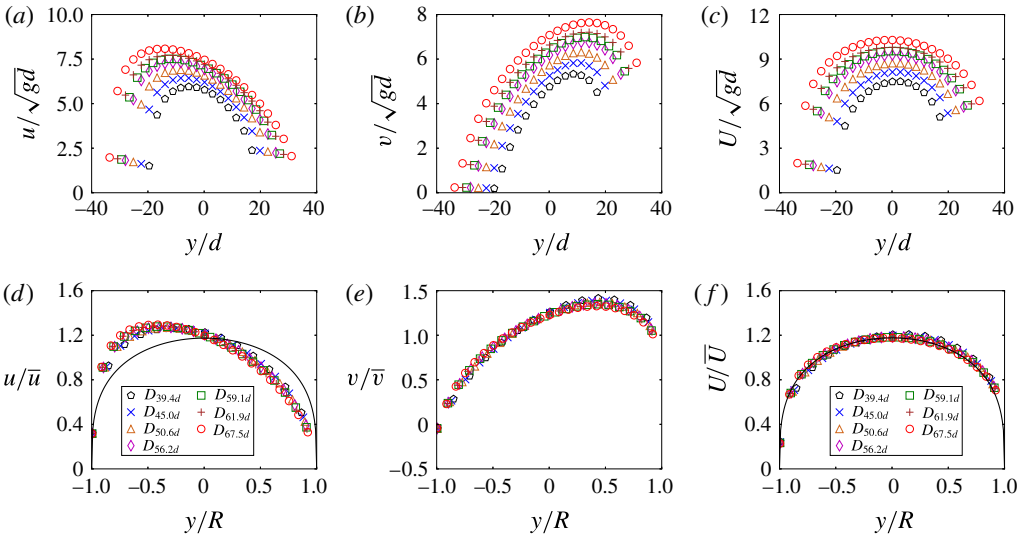

FIGURE 18. (Colour online) Two-dimensional continuum simulation (*a*,*d*) horizontal velocity (*b*,*e*) vertical velocity and (*c*,*f*) norm of the velocity, (*a–c*) normalised by $\sqrt{gd}$ versus y/d and (*d–f*) normalised by the mean value versus y/R, the full lines in (*d*,*f*) represent equation (A 5) with $\nu_v = 0.31$.

Figure 19(*a–c*) shows the mean value of the horizontal and vertical velocities and of the norm of the velocity, normalised by $\sqrt{gL}$ versus the dimensionless outlet diameter D/d for two particles diameters $d = L/30$ and $d = L/90$. Clearly these mean velocities depend on the outlet size D, but also on the particle diameter d. Following the discrete simulation study we have plotted in figure 19(*d–f*) these velocities made dimensionless with $\sqrt{gD}$ versus D/d. The data corresponding to the mean horizontal velocity (respectively to the mean norm) are reasonably well adjusted by (A 7) with the fitting parameters $\beta = 0.05$, $\xi_u = 0.78$ and $\alpha_u = 0.25$ (respectively $\xi_U = 1.06$ and $\alpha_U = 0.28$). The value of β is sensibly lower than the value obtained experimentally or in the discrete simulation. However the same tendency than observed in the discrete simulation is recovered. This is not the case for the mean vertical velocity for which the data do not follow the asymptotic behaviour in $\sqrt{gD}$. However this velocity is not involved in the flow rate and the (A 9) using the fitting parameters predicts well the flow rate, see the full line in figure 17(*b*).

Finally we have done the same analysis in the pseudo-3-D continuum simulation, in the regime controlled by the side wall friction. Figure 20(*a*) presents the profile of the horizontal velocity at the outlet for various D. In this regime, the profiles present the same asymmetric shape than in the Hagen–Beverloo profile, nevertheless the velocity does not seem to depend on D anymore. Figure 20(*b*) shows the mean horizontal velocity, normalised by $\sqrt{gW}$ versus W/d for data corresponding to the second regime, $D/W > 3$. Clearly we do not observe the geometrical function as suggested by the experimental results. This is not surprising as the flow is not solved throughout the silo width, thus the I number is not expected to play any role in this direction.

To conclude this section, we found that a dependency on the particle diameter is observed in the 2-D continuum simulation, that the velocity profiles are self-similar when varying the outlet length, and that the mean horizontal velocity tends

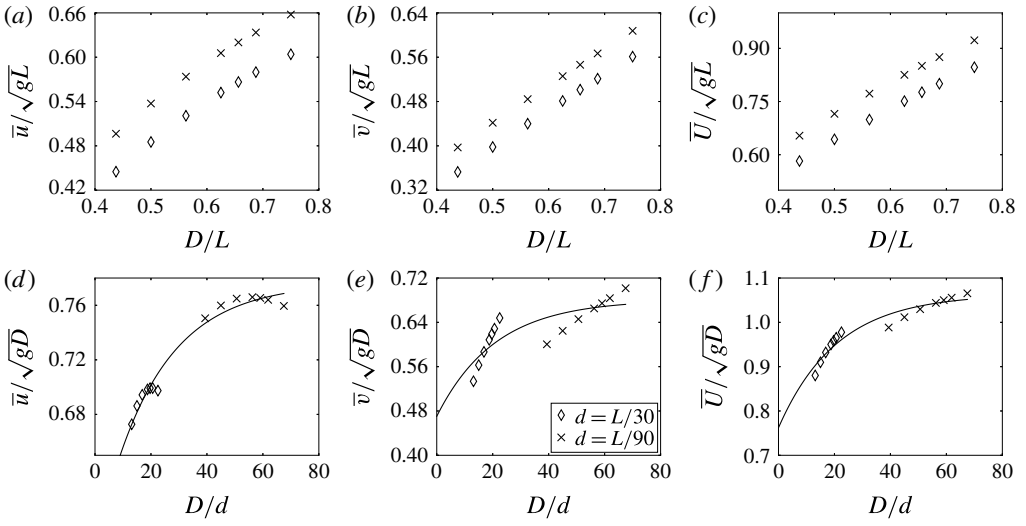

FIGURE 19. Two-dimensional continuum simulation: (*a*,*d*) horizontal velocity, (*b*,*e*) vertical velocity and (*c*,*f*) norm of the velocity normalised in (*a–c*) by $\sqrt{g\overline{L}}$ versus D/L and normalised in (*d–f*) by $\sqrt{g\overline{D}}$ versus D/d for two particles diameters. The full lines in (*d–f*) represent equation (A 7) with the fitting parameters $\beta = 0.05$, $\xi_u = 0.78$, $\alpha_u = 0.25$, $\xi_v = 0.68$, $\alpha_v = 0.31$, $\xi_U = 1.06$ and $\alpha_U = 0.28$ obtained using the least-squares method.

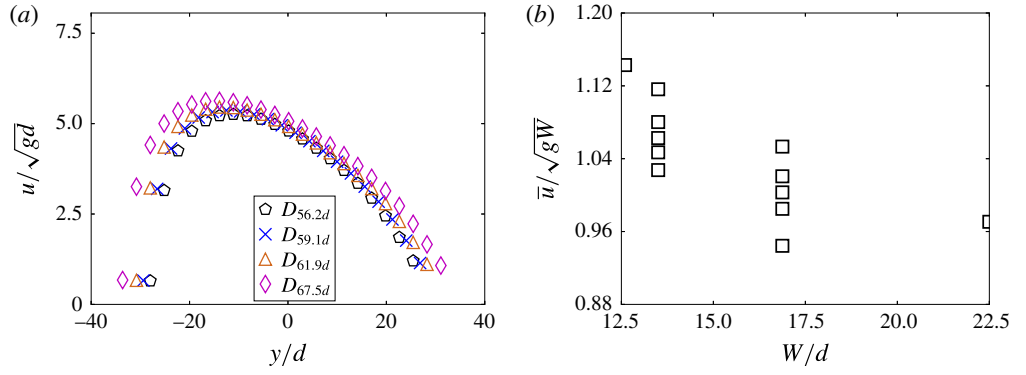

FIGURE 20. (Colour online) Pseudo-3-D continuum simulation. (*a*) Horizontal velocity normalised by $\sqrt{gd}$ versus y/d at the outlet for different D and $W = 13.5d$; (*b*) mean horizontal velocity normalised by $\sqrt{gW}$ for $D/W > 3$.

asymptotically towards $\sqrt{g\overline{D}}$, contrary to the mean vertical velocity. This behaviour is well described by a geometrical function given by (A 7). However the profiles present a larger asymmetry than the one predicted by the 2-D discrete simulations. This can be due to the fact that the volume fraction has been assumed to be uniform, whereas the complete $\mu(I)$-rheology, that includes a $\phi(I)$ relation, would predict a dilation of a granular media when it is sheared. The dependency on the particle diameter for the regime controlled by the side walls is not correctly described by the pseudo-3-D continuum simulation which does not solve the flow in the silo width direction.

REFERENCES

AGUIRRE, M. A., GRANDE, J. G., CALVO, A., PUGNALONI, L. A. & GÉMINARD, J.-C. 2010 Pressure independence of granular flow through an aperture. *Phys. Rev. Lett.* **104**, 238002.

BENYAMINE, M., DJERMANE, M., DALLOZ-DUBRUJEAUD, B. & AUSSILLOUS, P. 2014 Discharge flow of a bidisperse granular media from a silo. *Phys. Rev.* E **90**, 032201.

BERTHO, Y., GIORGIUTTI-DAUPHINÉ, F. & HULIN, J.-P. 2003 Dynamical Janssen effect on granular packing with moving walls. *Phys. Rev. Lett.* **90** (14), 144301.

BEVERLOO, W. A., LENIGER, H. A. & VAN DE VELDE, J. 1961 The flow of granular solids through orifices. *Chem. Engng Sci.* **15**, 260–269.

CHOI, J., KUDROLLI, A. & BAZANT, M. Z. 2005 Velocity profile of granular flows inside silos and hoppers. *J. Phys.: Condens. Matter* **17**, S2533–S2548.

DAVIER, G. & BERTAILS-DESCOUBES, F. 2016 Nonsmooth simulation of dense granular flows with pressure-dependent yield stress. *J. Non-Newtonian Fluid* **234**, 15–35.

DUNATUNGA, S. & KAMRIN, K. 2015 Continuum modelling and simulation of granular flows through their many phases. *J. Fluid Mech.* **779**, 483–513.

JANDA, A., ZURIGUEL, I. & MAZA, D. 2012 Flow rate of particles through apertures obtained from self-similar density and velocity profiles. *Phys. Rev. Lett.* **108**, 248001.

JOP, P., FORTERRE, Y. & POULIQUEN, O. 2005 Crucial role of sidewalls in granular surface flows: consequences for the rheology. *J. Fluid Mech.* **541**, 167–192.

JOP, P., FORTERRE, Y. & POULIQUEN, O. 2006 A constitutive law for dense granular flows. *Nature* **441**, 727–730.

LAGRÉE, P.-Y. 2007 Interactive boundary layer in a Hele Shaw cell. *Z. Angew. Math. Mech.* **87** (7), 489–498.

LAGRÉE, P.-Y., STARON, L. & POPINET, S. 2011 The granular column collapse as a continuum: validity of a Navier–Stokes model with a $\mu(I)$-rheology. *J. Fluid Mech.* **686**, 378–408.

MEDINA, A., CABRERA, D., LÓPEZ-VILLA, A. & PLIEGO, M. 2014 Discharge rates of dry granular material from bins with lateral exit holes. *Powder Technol.* **253**, 270–275.

MEUNIER, P. & LEWEKE, T. 2003 Analysis and treatment of errors due to high velocity gradients in particle image velocimetry. *Exp. Fluids* **35** (5), 408–421.

MIDI, G. D. R. 2004 On dense granular flows. *Eur. Phys. J.* E **14** (4), 341–365.

PERGE, C., AGUIRRE, M. A., GAGO, P. A., PUGNALONI, L. A., TOURNEAU, D. L. & GÉMINARD, J. C. 2012 Evolution of pressure profiles during the discharge of a silo. *Phys. Rev.* E **85**, 021303.

POPINET, S. 2003 Gerris: a tree-based adaptive solver for the incompressible euler equations in complex geometries. *J. Comput. Phys.* **190** (2), 572–600.

POPINET, S. 2009 An accurate adaptive solver for surface-tension-driven interfacial flows. *J. Comput. Phys.* **228** (16), 5838–5866.

POPINET, S. 2013–2016 Basilisk C reference manual. http://basilisk.fr/Basilisk%20C.

RADJAI, F. & DUBOIS, F. 2011 *Discrete-Element Modeling of Granular Materials*. Wiley.

RUBIO-LARGO, S. M., JANDA, A., MAZA, D., ZURIGUEL, I. & HIDALGO, R. C. 2015 Disentangling the free-fall arch paradox in silo discharge. *Phys. Rev. Lett.* **114**, 238002.

SERRANO, D. A., MEDINA, A., CHAVARRIA, G. R., PLIEGO, M. & KLAPP, J. 2015 Mass flow rate of granular material flowing from tilted bins. *Powder Technol.* **286**, 438–443.

SHELDON, H. G. & DURIAN, D. J. 2010 Granular discharge and clogging for tilted hoppers. *Granul. Matt.* **12**, 579–585.

STARON, L., LAGRÉE, P.-Y. & POPINET, S. 2012 The granular silo as a continuum plastic flow: The hour-glass versus the clepsydra. *Phys. Fluids* **24**, 103301.

STARON, L., LAGRÉE, P.-Y. & POPINET, S. 2014 Continuum simulation of the discharge of the granular silo, a validation test for the μ(I) visco-plastic flow law. *Eur. Phys. J.* E **37** (1), 5.

TIGHE, B. P. & SPERL, M. 2007 Pressure and motion of dry sand: translation of Hagen's paper from 1852. *Granul. Matt.* **9**, 141–144.

ZHOU, Y., RUYER, P. & AUSSILLOUS, P. 2015 Discharge flow of a bidisperse granular media from a silo: discrete particle simulations. *Phys. Rev.* E **92**, 062204.